REPORT DOCUMENTATION PAGE

Form Approved
OMB No. 0704-01-0188

The public reporting burden for this collection of information is estimated to average 1 hour per response, including the time for reviewing instructions, searching existing data sources, gathering and maintaining the data needed, and completing and reviewing the collection of information. Send comments regarding this burden estimate or any other aspect of this collection of information, including suggestions for reducing the burden to Department of Defense, Washington Headquarters Services Directorate for Information Operations and Reports (0704-0188), 1215 Jefferson Davis Highway, Suite 1204, Arlington VA 22202-4302. Respondents should be aware that notwithstanding any other provision of law, no person shall be subject to any penalty for failing to comply with a collection of information if it does not display a currently valid OMB control number.
PLEASE DO NOT RETURN YOUR FORM TO THE ABOVE ADDRESS.

1. REPORT DATE (DD-MM-YYYY)	2. REPORT TYPE	3. DATES COVERED (From - To)
15-06-2007	REPRINT	

4. TITLE AND SUBTITLE

Evaluation of WRF performance for depicting orographically-induced gravity waves in the stratosphere

5a. CONTRACT NUMBER

5b. GRANT NUMBER

5c. PROGRAM ELEMENT NUMBER
62601F

6. AUTHORS

Douglas C. Hahn

5d. PROJECT NUMBER
1010

5e. TASK NUMBER
OT

5f. WORK UNIT NUMBER
A1

7. PERFORMING ORGANIZATION NAME(S) AND ADDRESS(ES)

Air Force Research Laboratory /RVBYA
29 Randolph Road
Hanscom AFB, MA 01731-3010

8. PERFORMING ORGANIZATION REPORT NUMBER

AFRL-RV-HA-TR-2008-1070

9. SPONSORING/MONITORING AGENCY NAME(S) AND ADDRESS(ES)

10. SPONSOR/MONITOR'S ACRONYM(S)
AFRL/RVBYA

11. SPONSOR/MONITOR'S REPORT NUMBER(S)

12. DISTRIBUTION/AVAILABILITY STATEMENT

Approved for Public Release; distribution unlimited.

13. SUPPLEMENTARY NOTES

14. ABSTRACT

Orographically-induced gravity(buoyancy) waves can propagate through the tropopause to the lower stratosphere causing disruptions to high altitude aircraft operations. To forecast this high altitude turbulence (HAT) in real time, there is a need to determine optimal model nesting, vertical resolution, upper boundary conditions and diffusion to be able to detect these situations. Besides investigating the abovementioned model options, the WRF-ARW will be closely configured to the operational version used by the Air Force Weather Agency (AFWA). To perform the model evaluation, a case from a field experiment conducted at the Observatoire de Haute-Provence (OHP) in southeastern France between 22 November and 5 December 2004 will be examined. Using a forecast initialized from 00 UTC 23 November, it will be determined how well waves generated by a north/south Mistral type flow over the French Alps north of OHP are represented by the model.

15. SUBJECT TERMS

Mountain waves   Gravity waves   High altitude turbulence   Numerical weather prediction

16. SECURITY CLASSIFICATION OF:			17. LIMITATION OF ABSTRACT	18. NUMBER OF PAGES	19a. NAME OF RESPONSIBLE PERSON
a. REPORT	b. ABSTRACT	c. THIS PAGE			Douglas C. Hahn
UNCL	UNCL	UNCL	UNL	9	19B. TELEPHONE NUMBER (Include area code)

Standard Form 298 (Rev. 8/98)
Prescribed by ANSI Std. Z39.18

Evaluation of WRF performance for depicting orographically-induced gravity waves in the stratosphere

Douglas C. Hahn

Air Force Research Laboratory, Hanscom AFB, MA

1. Introduction

Orographically-induced gravity (buoyancy) waves can propagate through the tropopause to the stratosphere causing disruption to high altitude aircraft operations. High altitude turbulence (HAT) was first researched using U-2 aircraft in the mid-1960s and reported by Crooks (1965). He observed that HAT from mountain wave activity was more severe than turbulence associated with jet streams or convective activity. A few years later a severe downslope windstorm and turbulence event along the front range of the Rocky Mountains in Colorado was analyzed and reported by Lilly and Zipser (1972). Klemp and Lilly (1975) and Lilly (1978) concluded that this event on 11 January 1972 was precipitated by mountain wave activity occurring in the vicinity.

Klemp and Lilly (1978) consequently developed a two-dimensional hydrostatic model to simulate this case and compared their results to the linear analytic approach developed by Long (1953) and a linear approach used in Klemp and Lilly (1975). They concluded that there are two important requirements to modeling real data cases; without control over internal dissipation and the inclusion of a radiative upper boundary condition (UBC), predicted wave response would be unstable or over damped. Unstable or over damped gravity waves would, in turn, lead to incorrectly predicted vertical momentum flux, surface wind amplitude and vertical structure of all fields.

Not until Clark, et al. (1994) did anyone attempt to simulate a Colorado windstorm with a full three dimensional non-hydrostatic mesoscale model using high horizontal and vertical resolutions. Their simulations successfully predicted the strong windstorm and associated gravity wave breaking event, but the timing and location were not predicted well. Their work successfully proved that a mesoscale model could capture the basic structures of these events. However, the model, described by Clark and Hall (1991, 1996), is primarily used in studying microphysical processes and cloud formation, and has not been widely used as a general forecast model.

Typical non-hydrostatic three dimensional mesoscale models used for forecasting tropospheric weather usually have model tops defined in the lowest part of the stratosphere with a concentration of model levels in the tropopause and below. Doyle, et al. (2000) compared a number of common mesoscale models in two dimensions for the 11 January 1972 Boulder windstorm case using highly simplified topography and similar horizontal and vertical grid spacing at high resolution. It was concluded that all of the models possessed gravity wave breaking predictability. Furthermore, upper level wave breaking was shown to be sensitive to the vertical grid spacing, implying that the vertical resolution used in prognostic models was insufficient in resolving most upper level gravity wave propagation and breaking processes.

In this paper, the Weather Research and Forecasting (WRF) model with the Advanced Research WRF (ARW) core (Skamarock et al., 2005) version 2.1.1 is used to study the effects of including an upper boundary condition and the elimination of vertical velocity damping typically used for forecast stability in operational mode. Prior to the current version, WRF-ARW 2.2, upper boundary conditions were not recommended for application in real data simulations. Without an upper boundary condition, gravity waves which would reach the stratosphere would be mishandled at the top of the model and contaminate the model domain leading to a noisy and incorrect solution for depicting gravity waves there. Vertical velocity damping in WRF is typical of numerical diffusion

Corresponding author address: Douglas C. Hahn, AFRL/VSBYA, 29 Randolph Rd., Hanscom AFB, MA 01731-3010; email <Douglas.Hahn@hanscom.af.mil>

used to keep operational models stable and can also be a detriment to capturing HAT generated by gravity waves and their breaking.

Using WRF-ARW settings similar to those used by the Air Force Weather Agency (AFWA), the operational vertical grid spacing will be compared to a finer vertical resolution grid spacing combined with a higher specified model top. Some of this research closely parallels that reported by Koch, et al. (2006). However this paper addresses the needs of the Air Force within the WRF framework used by AFWA. Koch, et al. (2006) discusses relevant information to this study and the reader should refer to that paper for in depth background material.

2. Case Study

For this evaluation, a case was chosen from a field campaign conducted at the Observatoire de Haute Provence (OHP) in southeastern France from 22 November to 5 December 2004. OHP is located in the southern foothills of the French Alps with the Rhône Valley to the west. The Rhône Valley is bordered by the Massif Central to the west and the Alps to the east. Observations were made using thermosonde measurements, taken in parallel with generalized scintillation detection and ranging (SCIDAR) (Fuchs, et al, 1998) measurements at OHP. Thermosondes measure turbulence directly via the temperature structure function (C_t^2) described in Brown, et al. (1982).
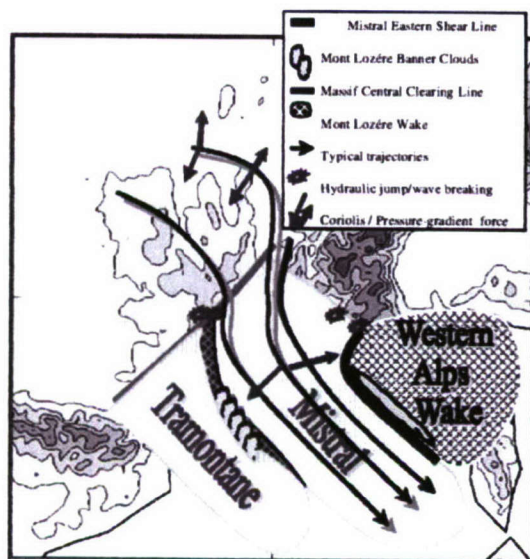

Fig. 1. Summary diagram depicting features of the mistral wind (from Jiang, et al., 2003).

This area is known for the Mistral wind which is characterized by strong surface winds in the Rhône Valley enhanced by air funneling into the valley from the Alps and Massif Central. When these winds are aided at 500 hPa by a ridge (or anti-cyclone) over Western Europe and a trough (or cyclone) over Eastern Europe they can lead to gravity waves generated by the topography as in Jiang, et al. (2003). Fig. 1, taken from Jiang, et al. (2003) summarizes the features of the Mistral.
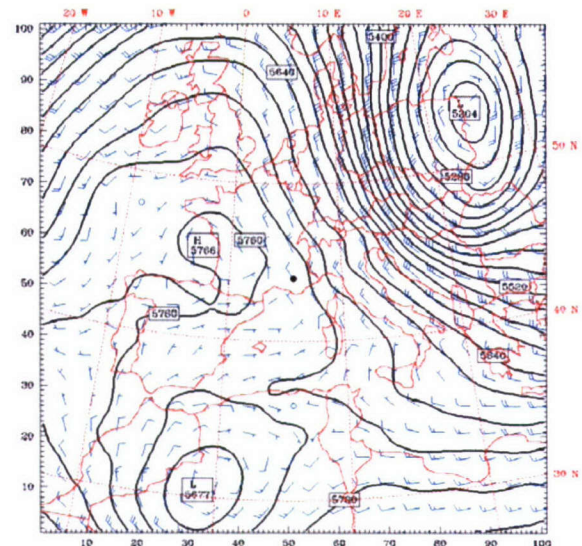

Fig. 2. Geopotential height (m) contours for 500 hPa pressure surface from GFS analysis valid 0000 UTC 24 November 2004. The point in the center of the plot is the location of OHP.

What can be characterized as a "light" Mistral was observed on 23-24 November 2004. Fig. 2 shows the 500 hPa geopotential height pattern at 0000 UTC 24 November 2004 from the GFS analysis as initialized on the 36 km ARW domain. The pattern is similar to the one documented in Jiang, et al. (2003) for the Mesoscale Alpine Programme (MAP) Intensive Observing Period (IOP) 15 which produced gravity waves. The current case differs from MAP IOP 15 because the typical ridge over Western Europe was embedded with a small closed off low over NW Africa and the trough over Eastern Europe was located further NE than usual. At the surface (not shown), the typical "Genoa low" associated with the Mistral formed near the Riviera as described in Guénard, et al. (2005). However, the current case did not produce a surface low as strong as in a typical Mistral.
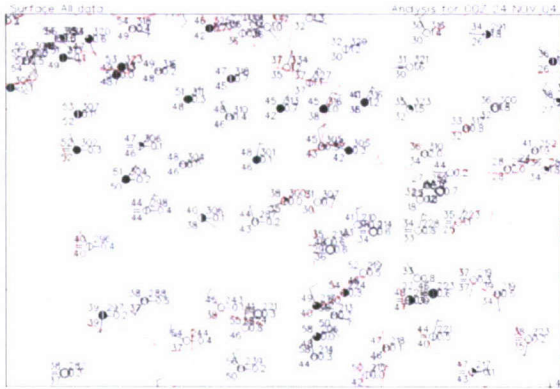
Fig. 3. Surface observations for Europe at 0000 UTC 24 November 2004 (courtesy Plymouth State Weather Center).

The SCIDAR measurements and thermosonde data confirmed optical turbulence at a height of 13-14 km on the night of 23-24 November 2004. In Fritts, et al. (2003) it is shown that thermal dissipation, associated with optical turbulence, and turbulent kinetic energy dissipation, associated with mechanical turbulence, are closely linked together in vigorous gravity wave breaking events. The observed turbulence could not be explained by either convection or extreme wind shear (due to wind speed, although some directional shear was present). Surface observations (Fig. 3) show that convection was not present during the period and radiosonde data (not shown) does not depict an unusually strong jet near the tropopause.

3. Numerical Simulations

As mentioned previously, WRF-ARW version 2.1.1 was used to perform the forecasts used in this evaluation. The model was configured to AFWA basic settings used on the Joint Operational Testbed in July 2005. When WRF-ARW version 2.1.2 was released in January 2006, that model was considered, but the published changes from version 2.1.1 appeared to be of minimal impact to the AFWA configuration that was already operating on the target computer. Two model runs were configured to test the sensitivity of WRF to upward propagating gravity waves; a control based on the standard AFWA ARW model choices and a similar version of the ARW model with increased horizontal and vertical resolution and the inclusion of an upper boundary condition (UBC).

The AFWA control ARW model used a horizontal domain resolution of 45 km with inner nests of 15 and 5 km and 42 vertical levels to a model top of 50 hPa. The enhanced resolution ARW version consisted of a 36 km domain and inner nests of 12, 4 and 1.3 km with 82 vertical levels and the model top set to 10 hPa. The horizontal grids for both model configurations were centered on the region of interest for the case study. The runs were made using two-way nesting and feedback from the nests to the parent grids with a smoothing-desmoothing feedback option.

Modifications were made to WRF to use a diffusive damping layer as a UBC for the enhanced ARW model. The UBC is described as a gravity wave absorbing layer in Skamarock, et al. (2005) and follows the Klemp and Lilly (1978) formula to gradually increase eddy viscosities to a maximum at the model top. It is controlled in the model by choosing the depth of the damping layer and an appropriate damping coefficient. Without a sufficient depth to the damping layer, the gravity waves would be subject to large viscosity variations at the top of the model. If the damping coefficient chosen is too large or too small, wave reflections could occur from the damping layer. A 5 km damping depth was used for all enhanced ARW model simulations since a deeper layer would intrude on a greater part of the model in the stratosphere. While the damping depth was constant for enhanced ARW model forecasts, the damping coefficient was tested with values of 0.01, 0.04 and 0.08.

Spatial dissipation in both model runs use second order diffusion on coordinate surfaces with vertical eddy viscosity computed from the planetary boundary layer (PBL) parameterization. The horizontal eddy viscosity is determined from the horizontal Smagorinsky first-order closure approach. Default values for the time-stepping filters were used for both models. In order to test the impact of vertical velocity damping (w-damping) on the vertically propagating gravity waves, time steps were reduced within the enhanced resolution version of WRF-ARW to attempt to avoid a violation of the vertical CFL criterion which would also allow w-damping to be turned off. Vertical velocity damping could unnecessarily suppress strong updrafts or downdrafts associated with significant gravity wave propagation and breaking.

Finally, forecasts were initialized identically using the WRF Standard Initialization (WRFSI) package from the National Centers for Environmental Prediction (NCEP) 1° Global Forecast System (GFS) analyses and lateral boundary conditions were updated every six hours assuming a perfect prog approach.

4. Results

In order to verify that the enhanced resolution version of WRF-ARW can do better than the AFWA control at the tropopause and above, the 24 hour simulations valid at 0000 UTC 24 November were compared to the GFS analysis at the same time. Statistics in Fig. 4 show improvements over the AFWA control especially above 100 hPa. Total mean wind errors in Fig. 5 show that the RMSE of the total wind below 100 hPa in Fig. 4b are acceptable for the enhanced resolution ARW model.
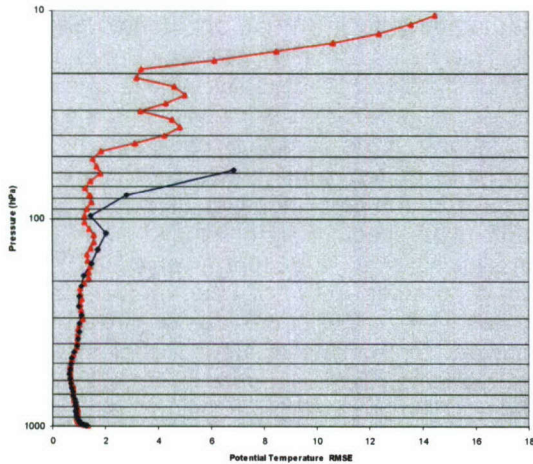

Fig. 4a. RMSE of potential temperature of simulation at 0000 UTC 24 November 2004 vs. GFS analysis. Blue profile represents AFWA control on 45 km grid and red profile represents increased resolution WRF on 36 km grid with inclusion of UBC. The UBC depth is roughly 10 hPa thick and begins around 20 hPa in chart.

Profiles were also extracted from the 36 km grid of the enhanced ARW model simulations along the balloon trajectories and compared directly with the high resolution radiosonde data. The radiosonde data was from a balloon released at 2335 UTC on 23 November. Fig. 6 shows that except for the fine details of the radiosonde temperature and wind profiles, the smooth profiles of the enhanced ARW model follow the radiosonde profiles on average. The wind profiles from the radiosonde appear noisy due to the high temporal resolution of the data and may be indicative of gravity wave activity

occurring over OHP. The AFWA control was not used in this comparison since the top of that model was too low to compare with the radiosonde data above the tropopause.
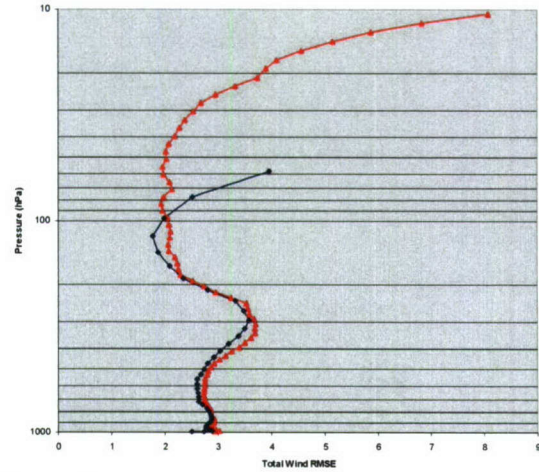

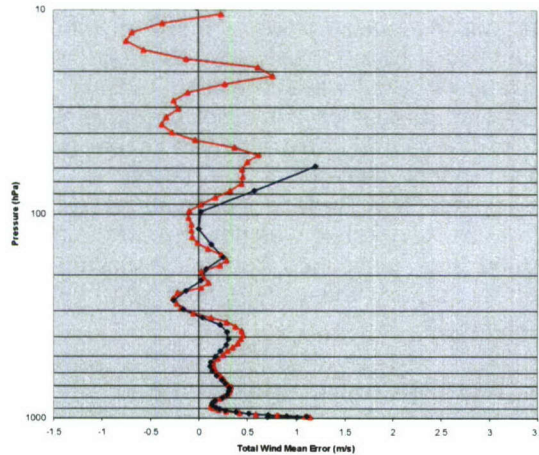Fig. 4b. Same as in 4a, except for total wind speed.

Fig. 5. Mean wind error of simulation at 0000 UTC 24 November 2004 vs. GFS analysis. Profiles are represented by the same colors as in Fig. 4.

From these comparisons it can be deduced that the enhanced resolution version of WRF-ARW performed adequately on the 36 km grid with 82 vertical levels. Following this assessment, simulations on the 1.3 km innermost nest (Fig. 7) were evaluated on how well the enhanced ARW model was able to resolve the gravity waves and associated turbulence observed in this case. The sensitivity of the enhanced ARW model to different values of damping coefficient in the UBC was also evaluated.

Tests were performed with and without vertical velocity damping (w-damping) in the

enhanced resolution ARW, but the results led to only small differences in the strength of the forecasted vertical velocity. In order to test w-damping, the timesteps on the 1.3 km grid were chosen to be 5 seconds to avoid vertical CFL instability. Even though the impact of including w-damping was minimal, it was not used for the tests involving the UBC in the interest of eliminating one source of model dissipation.
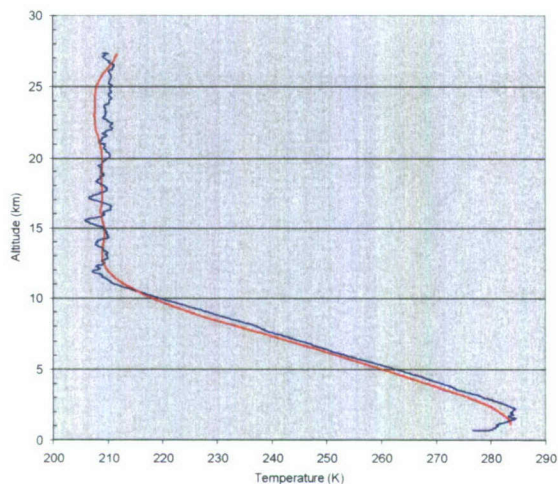

Fig. 6a. Comparison between radiosonde (blue) at 2335 UTC 23 November 2004 and model simulation (red) profile of temperature at 24 hours. Model profile was extracted spatially and temporally from 36 km grid data.
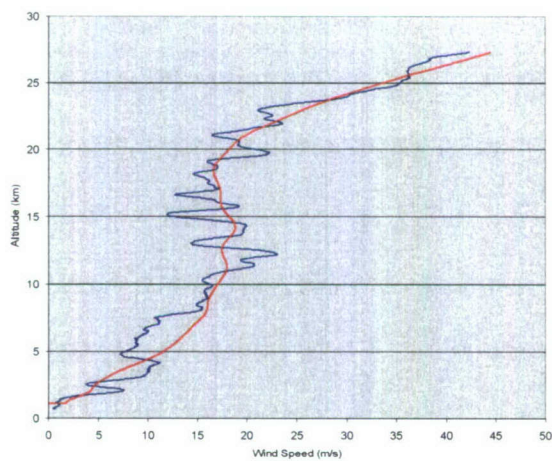

Fig. 6b. Same as in 6a, except for wind speed.

Since we are interested in stratospheric gravity waves and we know that gravity waves were present near the surface during the OHP 2004 case (Fig. 8), only forecast data above the tropopause were evaluated. Fig. 9 illustrates that greater gravity wave activity appears to be occurring over the Alps along the border between Italy and Switzerland at this time.

Since observation data for turbulence was not available for this area, only the weaker case near the center of the horizontal grid in Fig. 7 was evaluated, however attention to the structure of the vertical velocity field should still be given for the entire grid window.
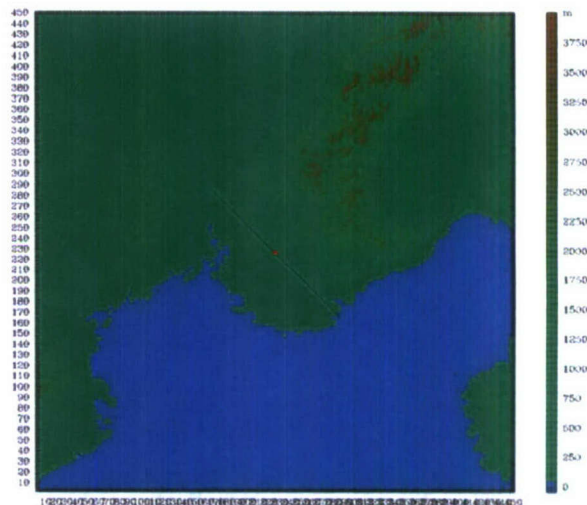

Fig. 7. Map of Southeastern France over the Provence Region. Red bullet indicates the location of OHP. The northwest to southeast line represents the location of the vertical cross sections in Figs. 8 and 10.
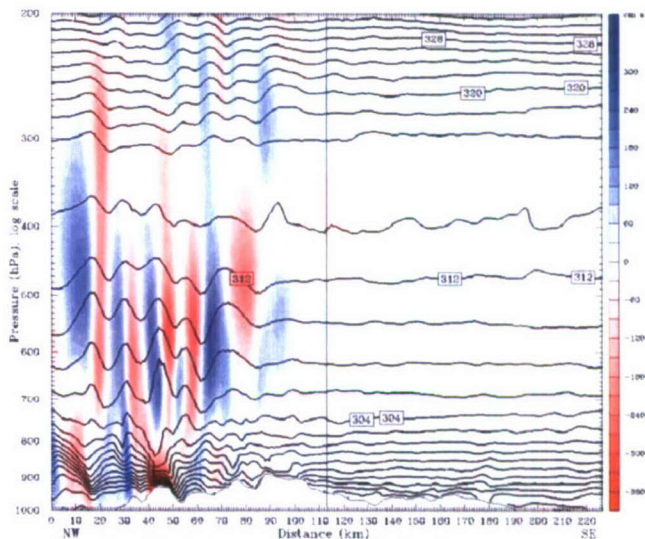

Fig. 8. Vertical cross section indicating orographically generated gravity waves near the surface in the vertical velocity (cm s^{-1}, color contours) and potential temperature (K, line contours) fields (location depicted in Fig. 7 above). Vertical line at center is location of OHP.

The 24 hour forecast vertical velocity field at 13 km was chosen since this was the approximate time and area thermosonde observations were detecting turbulent activity near OHP. The addition of the gravity wave

absorbing UBC (Fig. 9b) does subtly show that less noise is generated in the vertical velocity fields, especially downstream towards and over the Mediterranean Sea. Nevertheless, there is a weak gravity wave structure present in the horizontal cross section of the vertical velocity field in the Provence region over southeastern France.
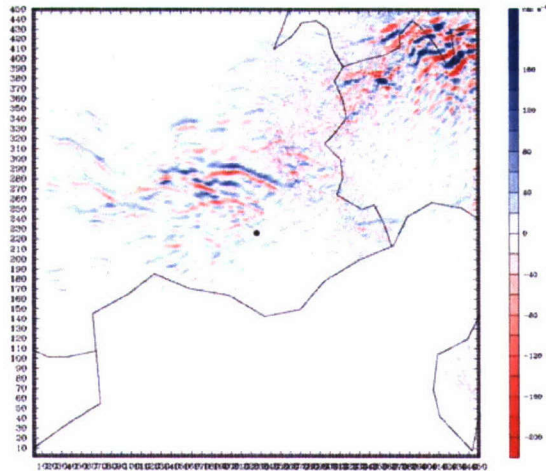

Fig. 9a. Horizontal cross section at 13 km of the enhanced resolution ARW without the UBC. This is a 24 hour forecast of vertical velocity (cm s^{-1}) valid at 0000 UTC 24 November.
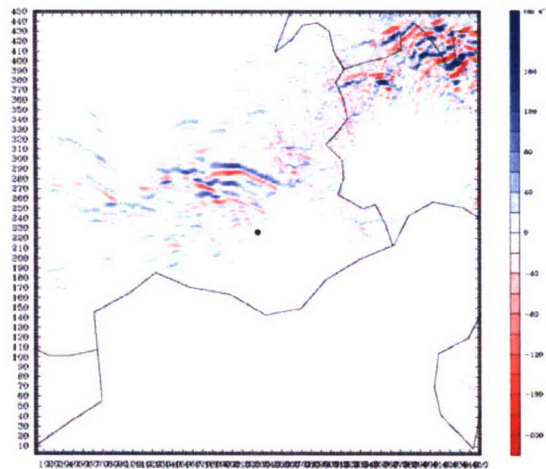

Fig. 9b. Same as in 8a, except with the inclusion of the gravity wave absorbing UBC. Damping coefficient (γ_g) was set to 0.01.

Evaluating vertical cross sections along a northwest to southeast line bisected by the location of OHP (marked by line in Fig. 7), it can be seen that several locations above 13 km northwest of OHP show some type of gravity wave activity. Fig. 10a is a vertical cross section of the enhanced resolution ARW model using the absorbing UBC and a damping coefficient

(γ_g) of 0.01. There are three locations above the 13 km level in Fig. 10a where it appears that waves may be near breaking; one small area between 15 and 16 km, another near 17 km and a third around 21 km. At each location, the upward vertical velocities are the strongest and the potential temperature contours are near vertical, typical signs indicating areas of possible wave breaking. A wave pattern is evident in the vertical velocity field with wavelengths on the order of 10 km.
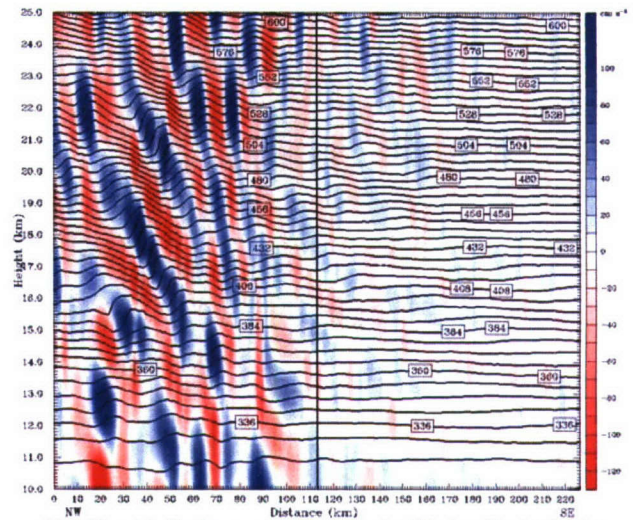

Fig. 10a. Vertical cross section of color filled vertical velocity (cm s^{-1}) contours and contours of potential temperature (K) for the enhanced WRF model forecast at 24 hours, valid at 0000 UTC 24 November and using a UBC damping coefficient of 0.01. Vertical line in the center of the graph is the location of OHP.
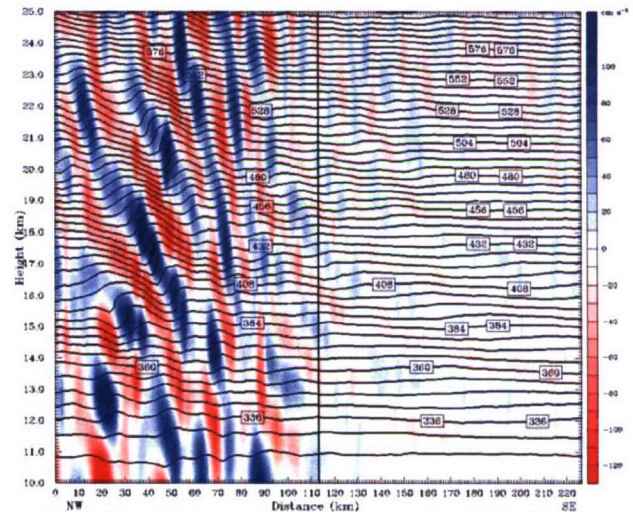

Fig. 10b. Same as in 10a. except with UBC damping coefficient of 0.04.

To evaluate the sensitivity of the UBC to different values of damping coefficient, Fig. 10b and 10c are shown with coefficients of 0.04 and 0.08, respectively. The largest difference in the vertical cross sections appears between the version using a coefficient of 0.01 and that using 0.04. Noise in the vertical velocity field is reduced in Fig. 10b over 10a, especially in the area southeast of OHP. The wave structure based on the maximum vertical velocities appears more coherent and less fractured to the northwest.
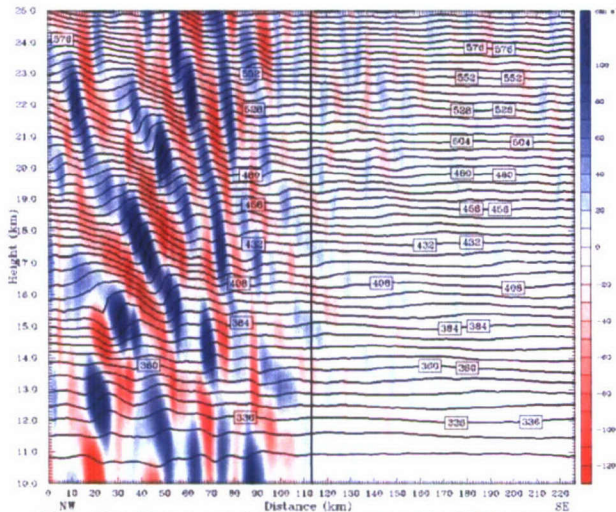

Fig. 10c Same as in 10a except with UBC damping coefficient of 0.08.

Finally, comparing Fig. 10c with Fig. 10b, there is no real improvement in the noise of the vertical velocity field. It can be concluded that increasing the damping coefficient beyond 0.04 will not improve the effectiveness of the UBC and may even thwart it.

5. Summary and Conclusions

Simply increasing the model top and the vertical resolution of the ARW model the simulations were improved in the stratosphere. Specifically, forecast errors were reduced above 100 hPa over the control AFWA ARW model. The enhanced resolution ARW model compared satisfactorily with radiosonde data even though the model profiles were highly smoothed.

There is evidence in the cross sections that gravity wave activity above the tropopause is occurring in the enhanced resolution ARW model simulations. Forecasted strength is most likely weaker than the actual observations. Unfortunately it appears that greater gravity

wave activity and possible breaking was northeast of OHP during the SCIDAR and thermosonde observations. Although it was not presented, greater gravity wave activity appeared in the forecast over OHP prior to 0000 UTC 24 November. This disconnect may have been due in part to measurements focusing on optical (from thermal dissipation) turbulence, whereas optical turbulence occurs in thin layers usually as remnants of prior mechanical turbulence events as a result of wave breaking.

It is unclear how well increasing the damping coefficient above 0.04 improves the gravity wave absorbing UBC and subsequently the wave structures in the stratosphere. However, by including the UBC, the amount of noise within the vertical velocity field is incrementally decreased. Even with a Rayleigh damping layer now available in ARW version 2.2, better UBC choices may be needed. In Durran (1999) there is a discussion of gravity wave absorbing UBCs and their problems even though they have been widely used for several years in models. One possible solution to current UBC problems is the perfectly matched layer (PML) approach developed by Berenger (1994). This UBC has been used by Hayder, et al. (1999) and Navon, et al. (2004) in simplified shallow water models, however, successful implementation in existing three dimensional mesoscale models has not been reported.

The amount of computational time required to produce forecasts at these higher horizontal and vertical resolutions would be an impediment for operational forecasting. In addition, you would need to have prior knowledge of where these gravity wave events were occurring in order to capture them with higher resolution inner nests. One possible solution is to use the Real-Time Turbulence Model framework described by Kaplan, et al. (2006) which automatically nests to the potential areas of turbulence. Another prospective solution is to dynamically adjust the grid size in the model to give greater resolution to the areas where turbulence is likely, as in Xiao, et al. (2005). Both of these methods are currently being tested using the WRF-ARW model.

In conclusion, even with numerous problems, WRF-ARW is capable of capturing gravity wave events that lead to the waves penetrating the tropopause and propagating into the stratosphere. In the future, we hope to continue testing WRF-ARW on a new case

where turbulence directly impacted a NASA ER-2 training flight over southwestern Wyoming in February 2006.

6. References

Berenger, J.-P., 1994: A perfectly matched layer for the absorption of electromagnetic waves. *J. Comput. Phys.*, **114**, 185-200.

Brown, J. H., R. E. Good, P. M. Bench and G. Faucher, 1982: Sonde measurement for comparative measurements of optical turbulence. Air Force Geophysics Laboratory Technical Report, AFGL-TR-82-0079. 46 pp. ADA118740

Clark, T. L., and W. D. Hall, 1991: Multi-domain simulations of the time dependent Navier Stokes equation: Benchmark error analyses of nesting procedures. *J. Comput. Phys.*, **92**, 456-481.

_____, and W. D. Hall, 1996: On the design of smooth, conservative vertical grids for interactive grid nesting with vertical stretching. *J. Appl. Meteor.*, **35**, 1040–1046.

_____, W. D. Hall and R. M. Banta, 1994: Two- and three-dimensional simulations of the 9 January 1989 severe Boulder windstorm: Comparison with observations. *J. Atmos. Sci.*, **51**, 2317-2343.

Crooks, W. M., 1965: High altitude clear air turbulence. Air Force Flight Dynamics Laboratory, Research and Technology Division Technical Report, AFFDL-TR-65-144 (Lockheed Report 18794), 130 pp. AD0474616.

Doyle, J. D., and Coauthors, 2000: An intercomparison of model-predicted wave breaking for the 11 January 1972 Boulder windstorm. *Mon. Wea. Rev.*, **128**, 901-914.

Durran, D. R., 1999: *Numerical Methods for Wave Equations in Geophysical Fluid Dynamics.* Springer-Verlag, 465 pp.

Fritts, D. C., C. Bizon, J. A. Werne and C. K. Meyer, 2003: Layering accompanying turbulence generation due to shear instability and gravity-wave breaking. *J. Geophys. Res.*, **108**, 8452-8464.

Fuchs, A., M. Tallon and J. Vernin, 1998: Focusing on a turbulent layer: Principle of the "Generalized SCIDAR". *Publ. Astron. Soc. Pac.*, **110**, 86-91.

Guénard, V., G. Tedeschi, P. Drobinski and J. L. Caccia, 2005: Wave breaking over local topography during the MAP IOP 15 mistral event: Observations and high-resolution numerical simulations. Preprints, *28th Int. Conf. Alpine Meteorology*, Zadar, Croatia, WMO.

Hayder, M. E., F. Q. Hu and M. Y. Hussaini, 1999: Towards perfectly absorbing boundary conditions for Euler equations. *AIAA J.*, **37**, 912-918.

Jiang, Q., R. B. Smith and J. D. Doyle, 2003: The nature of the mistral: Observations and modelling of two MAP events. *Q. J. R. Meteorol. Soc.*, **129**, 857–875.

Kaplan, M. L., and Coauthors, 2006: Characterizing the severe turbulence environments associated with commercial aviation accidents. A real-time turbulence model (RTTM) designed for the operational prediction of hazardous aviation turbulence environments. *Meteorol. Atmos. Phys.*, **94**, 235-270.

Klemp, J. B., and D. K. Lilly, 1975: The dynamics of wave-induced downslope winds. *J. Atmos. Sci.*, **32**, 320-339.

_____, and D. K. Lilly, 1978: Numerical simulation of hydrostatic mountain waves. *J. Atmos. Sci.*, **35**, 78-107.

Koch, S. E., L. R. Bernardet, B. D. Jamison and J. M. Brown, 2006: Modeling of mountain waves in T-Rex. Preprints, *12th Conf. on Mountain Meteorology.* Santa Fe, NM, Amer. Meteor. Soc.

Lilly, D. K., 1978: A severe downslope windstorm and aircraft turbulence event induced by a mountain wave. *J. Atmos. Sci.*, **35**, 59-77.

_____, and E. J. Zipser, 1972: The front range windstorm of 11 January 1972—a meteorological narrative. *Weatherwise*, **25**, 56-63.

Long, R. R., 1953: Some aspects of the flow of stratified fluids. I. A theoretical investigation. *Tellus*, **5**, 42-58.

Navon, I. M., B. Neta and M. Y. Hussaini, 2004: A perfectly matched layer approach to the linearized shallow water equations models. *Mon. Wea. Rev.*, **132**, 1369-1378.

Skamarock, W. C., et al., 2005: A description of the Advanced Research WRF version 2. NCAR Technical Note, NCAR/TN-468+STR, 98 pp. <http://www.mmm.ucar.edu/wrf/users/docs/arw_v2.pdf>

Xiao, X., D. S. McRae and H. A. Hassan, 2005: Dynamically resolved simulation of atmospheric features and turbulence – Initial results. Preprints, 43rd *AIAA Aerospace Sciences Meeting and Exhibits*, Reno, NV, AIAA-2005-265.